Received: 19 January 2022 | Revised: 4 August 2022 | Accepted: 5 December 2022

DOI: 10.1002/jbm.a.37486

RESEARCH ARTICLE

Implant surface physicochemistry affects keratinocyte hemidesmosome formation

Michail Raptopoulos[1,2] | Nicholas G. Fischer[1] | Conrado Aparicio[1,3,4]

[1]Minnesota Dental Research Center for Biomaterials and Biomechanics, University of Minnesota, Minneapolis, Minnesota, USA

[2]Division of Periodontology, Department of Developmental and Surgical Sciences, University of Minnesota, Minneapolis, Minnesota, USA

[3]Basic and Translational Research Division, Department of Odontology, UIC Barcelona – Universitat Internacional de Catalunya, Barcelona, Spain

[4]IBEC - Institute for Bioengineering of Catalonia, BIST-Barcelona Institute of Science and Technology, Barcelona, Spain

Correspondence
Conrado Aparicio, Department of Odontology, UIC Barcelona - Universitat Internacional de Catalunya, Barcelona, Spain.
Email: cjaparicio@uic.es

Funding information
National Institute of Dental and Craniofacial Research, Grant/Award Numbers: F30DE029105, R01DE026117

Abstract

Previous studies have shown hydrophilic/hydrophobic implant surfaces stimulate/hinder osseointegration. An analogous concept was applied here using common biological functional groups on a model surface to promote oral keratinocytes (OKs) proliferation and hemidesmosomes (HD) to extend implant lifespans through increased soft tissue attachment. However, it is unclear what physicochemistry stimulates HDs. Thus, common biological functional groups (—NH_2, —OH, and —CH_3) were functionalized on glass using silanization. Non-functionalized plasma-cleaned glass and —H silanization were controls. Surface modifications were confirmed with X-ray photoelectron spectroscopy and water contact angle. The amount of bovine serum albumin (BSA) and fibrinogen, and BSA thickness, were assessed to understand how adsorbed protein properties were influenced by physicochemistry and may influence HDs. OKs proliferation was measured, and HDs were quantified with immunofluorescence for collagen XVII and integrin β4. Plasma-cleaned surfaces were the most hydrophilic group overall, while —CH_3 was the most hydrophobic and —OH was the most hydrophilic among functionalized groups. Modification with the —OH chemical group showed the highest OKs proliferation and HD expression. The OKs response on —OH surfaces appeared to not correlate to the amount or thickness of adsorbed model proteins. These results reveal relevant surface physicochemical features to favor HDs and improve implant soft tissue attachment.

KEYWORDS
attachment, hemidesmosome, implant, keratinocyte, organosilane, physicochemistry

1 | INTRODUCTION

The ability of a biomaterial surface to promote a specific cellular response is highly desired when devices are used for replacing critical organs of the human body, such as teeth.[1] Among other properties, surface wettability and electric charge are key properties repeatedly shown to influence cell adhesion, proliferation, and differentiation.[2] Bulk titanium (Ti) and its alloys have been the material of choice in dental (and orthopedic) implants because of the materials' mechanical strength and ability to osseointegrate.[3] However, despite Ti biocompatibility, implants mainly fail because of peri-implantitis, that is, infection of the peri-implant tissues that originates at the implant surface. On average, peri-implantitis occurs in 9.6% of implants and fuels an enormous economic burden on patients and the dental healthcare system.[4,5]

Recent attention has been given to the soft tissue around implants as an important factor for maintaining implant health.[6,7]

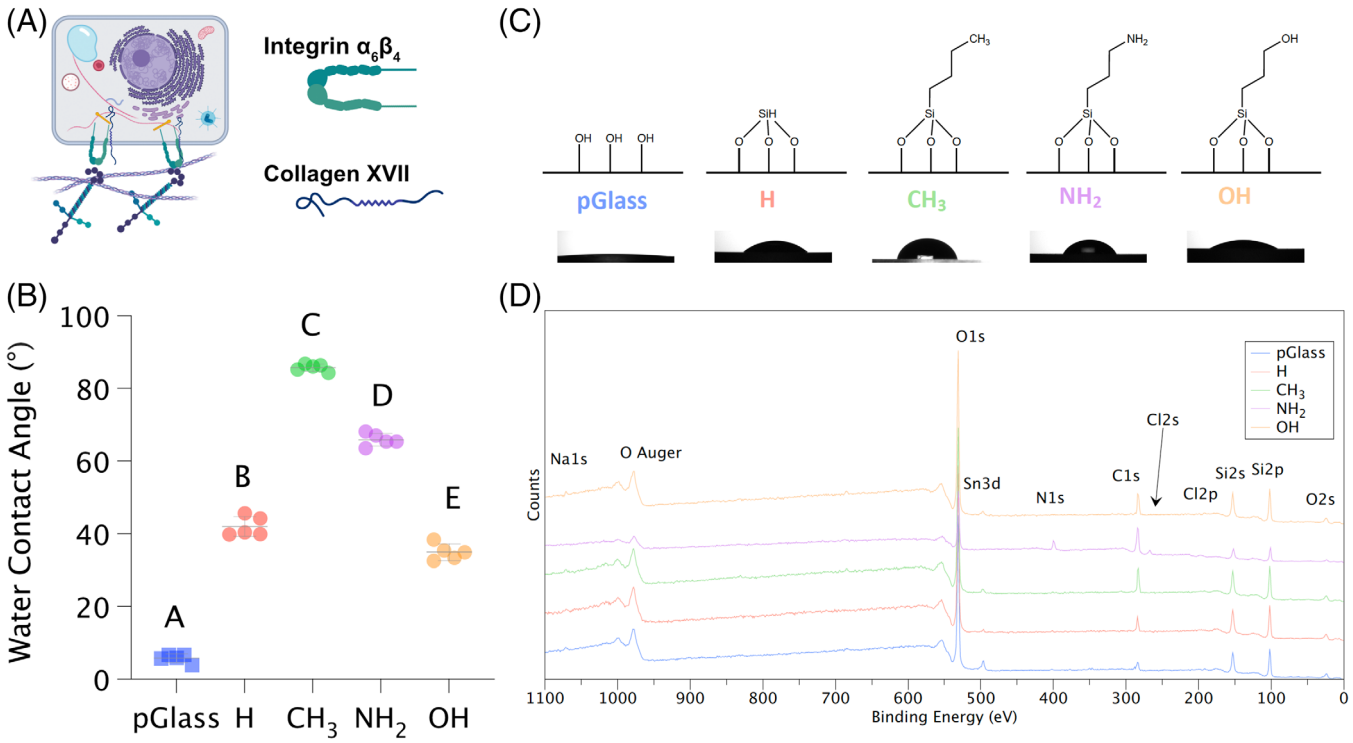

FIGURE 1 (A) Hemidesmosome structure, in particular, core components integrin $\alpha_6\beta_4$ and collagen XVII (COL17). (B) Water contact angles of control and modified glass surfaces. Dissimilar letters indicate statistically significant differences between groups. Error bars represent standard deviation ($n = 5$). (C) Chemical structures of organosilanes on glass surfaces. (D) X-ray photoelectron spectroscopy survey spectra of all tested surfaces ($n = 3$)

This interest is driven by well-reviewed deficiencies in antimicrobial and antibiotic strategies for treating infection rather than potentially preventing it.[8,9] Epithelial attachment around implants is ideally similar to that around teeth as teeth have far longer lifespans than implants.[10] However, while oral keratinocyte cells (OKs) attach to metallic abutments and form hemidesmosomes (HD) after 2–3 days of healing, like they do to natural teeth,[11] this attachment is weaker, with less HD formation, compared to natural teeth.[12,13] HD are cell adhesive structures formed solely by keratinocytes of the junctional epithelium directly abutting implants and are composed by three classes of proteins: cytoplasmic plaque proteins, transmembrane proteins and basement membrane-associated proteins of extracellular matrix (ECM).[14] Two key components of HD, that are also used as HD formation indexes, are integrin $\alpha_6\beta_4$ and collagen XVII (COL17). Integrin $\alpha_6\beta_4$ connects the ECM with the intracellular keratin cytoskeleton, while COL17 anchors HD into the lamina lucida of the basal membrane with its extracellular component[15–18] (Figure 1A). Absence of either of these abolishes HD formation and leads to fragility and destruction of the dermoepithelial junction.[19–21] Overall, upregulation of HD formation on dental implants is a promising route for preventing peri-implantitis through enhanced soft tissue attachment.

Previous studies have shown that coated Ti surfaces with peptides inspired by the ECM can increase the number of HDs.[22,23] Alternatively, controlling HD formation using physicochemical surface modifications is potentially advantageous given challenges, such as stability and cost, associated with more complex surface coatings like peptides and proteins.[24] As a result, many previous studies have attempted to increase our knowledge of cell interactions with physicochemically modified surfaces that, broadly, enhance cell adhesion.[25] However, these studies generally focused on the effects of implants on osseointegration by looking for ways to promote differentiation of stem cells to osteogenic cells on modified surfaces rather than HD formation.[26]

Previous studies conducted on silane-modified glass surfaces with human mesenchymal stem cells (MSCs) showed that, on the one hand, those cultivated on —NH_2 modified glass surfaces promoted focal adhesion formation together with osteogenic differentiation of MSCs. —COOH and —OH surfaces were related to chondrogenic differentiation and clean glass and —CH_3 surfaces maintained the stemness of the cells.[27,28] On the other hand, studies conducted with Chinese hamster ovary (CHO) cells, mouse embryonic fibroblasts (NIH/3T3) and, calf pulmonary artery endothelial cells showed that positively charged surfaces enhanced cell attachment indirectly by greater protein absorption.[29] As a result, strategies capable of affecting the electric charge and/or affecting the surface's wettability, have been used to create either hydrophilic or hydrophobic surfaces that stimulate and prevent cell adhesion, respectively.[1,29,30] Although surface wettability seems to determine the MSC response more than electric charge,[1] electric charge is key during the initial 2 h (sedimentation) of cell attachment to surfaces, when cells begin to form focal adhesions.[29,31]

It is known that epithelial cells around implants or abutments can adhere to partially prevent bacterial colonization and peri-implantitis[11,13]; this adhesion is stronger around smooth or finely grooved Ti surfaces with increased wettability.[11,32] However, wettability is a general phenomenon that may arise from different secondary forces at the surface/water interface. Further, protein adsorption usually mediates cell/surface interactions and is also guided by surface properties like polarity and charge.[11]

Overall, it is unclear what surface physicochemistry can promote HD formation and how well, or poorly, trends from other cell types, like MSCs, apply. Indeed, a recent meta-analysis aiming to discern ideal surface properties for soft tissue attachment concluded that meta-analysis of the data was not possible due to heterogeneity in the published study designs[33] A better understanding of keratinocyte proliferation and HDs through rationally designed modified surfaces could soundly inform implant design and provide support for a mechanistic description of the often-reported positive correlation between surface wettability and enhancement of soft tissue attachment around implants.[24]

The aim of our study was to assess OKs proliferation and HD formation cultivated on silane-modified glass surfaces with common biological functional groups of different polarity and charge (—H, —NH_2, —OH, and —CH_3). By identifying, the physical–chemical property(ies) that favor HD formation, bioinstructive abutment and implant surfaces could be engineered to promote strong and durable OKs attachment to implants and prevent peri-implantitis.

2 | MATERIALS AND METHODS

2.1 | Surface coatings

2.1.1 | Selected chemistries

Silanization was performed based on previous studies to modify the surface chemistry of glass disks with functional groups with different polarity and/or different charge.[34–36] Plasma-cleaned glass disks were used as control group for the material itself (pGlass). Using silanization, an unreactive terminal hydrogen was applied on plasma-cleaned glass disks serving as control for the coating process (—H). In the test groups, the modifications resulted in polar/positive/hydrophilic terminal —NH_2 surfaces (—NH_2), polar/neutral/hydrophilic —OH (—OH) and apolar/hydrophobic —CH_3 (—CH_3) under physiological conditions.[1,3,25,37] A negatively charged/polar functional group was not included in our final experimental design as synthesis of an analogous —COOH terminated organosilane was not possible.

2.1.2 | Silanization

All chemicals were used as received from Sigma-Aldrich unless otherwise noted. Borosilicate glass disks (Yuanbo Engineering Co. Ltd.) were activated by plasma cleaning (O_2 for 20 min, PDC-32G, Harrick Plasma) and immediately used. Activated samples were silanized by introducing 7.0 ml of anhydrous pentane into a N_2-saturated chamber with 0.6 ml of diisopropylethylamine (DIPEA), and depending on the modified surface, 0.91 ml of triethoxysilane for —H group, 1.16 ml (3-aminopropyl) triethoxysilane for —NH_2 group, 0.79 ml 3-(triethoxysilyl)-1-propanol for —OH group (Gelest) or 1.57 ml butyltriethoxysilane for —CH_3 (Gelest) for 1 h. Volumes were selected to maintain an equimolar relationship between silane and DIPEA. Periodic 2-min ultrasonication cycles were applied after every 10 min of reaction for a total of 1 h. After silanization, the samples were washed with ethanol, isopropyl alcohol, deionized water (DI) and acetone, and then dried with N_2 gas.[34–36] Samples were stored under desiccation until use.

2.2 | Surface characterization

2.2.1 | Elemental composition by X-ray photoelectron spectroscopy

A PHI 5000 VersaProbe III (ULVAC Inc.) X-ray photoelectron spectroscopy (XPS) along with a monochromatic Al Kα X-ray source (45°, 1486.6 eV, 50 W, sampling area; 200 μm diameter) were used for the elemental analysis. Results were collected using a step size of 1.0 eV with a pass energy of 280 eV. Charge compensation had to be used and was calibrated with the C1s signal located at 284.8 eV. Final surface elemental composition determination (as atomic composition [atomic %]) was performed using MultiPak (ULVAC Inc.) by subtracting (system optimized) peak areas from background.[35] At least 3 samples were tested per group.

2.2.2 | Water contact angle goniometry

Sessile drop contact angle measurements were performed using a contact angle analyzer (DM-CE1, Kyowa Interface Science) with appropriate software (FAMAS, Kyowa Interface Science). DI water was used as the wetting liquid with a drop volume of 2 μl.[26] The measurement was made after plasma activation and after silanization. Five samples were tested per group.

2.2.3 | Fourier transform infrared spectrometry

A Fourier transform infrared spectrometer (FTIR) (Nicolet iS50, Thermo Fisher Scientific) in attenuated total reflection mode (ATR-FTIR) was used to record spectra from 400 to 4000 cm^{-1} using an incremental step size of 2 cm^{-1}. Spectra were signal averaged from 8 scans; peaks of interest are shown.

2.3 | Oral keratinocyte response

2.3.1 | Keratinocyte cultivation and hemidesmosome formation

Immortalized human TERT-2/OKF-6 (OKs; BWH Cell Culture and Microscopy Core) OKs from normal tissue from the floor of the mouth

were cultured in defined keratinocyte serum-free medium (Gibco) with 1% penicillin/streptomycin (Gibco) antibiotics under standard conditions.[38] OKs were cultivated (2×10^4 per well for all experiments) for 1, 3, and 5 days based on previous work.[39] After each culture period, cells were fixed for 10 min using ice-cold methanol or 4% paraformaldehyde. Bovine serum albumin (BSA) in PBS (5%) was used to block fixed cells before immunofluorescence. Cells were probed with primary rabbit polyclonal antibody for COL17 ([critical late marker for HD assembly - methanol fixed] ab28440; Abcam; 1:500) and an antibody for Integrin β_4 ([ITGB4] critical early marker for HD assembly - paraformaldehyde fixed) (NB10065599; Novus Biologicals; 1:500) for 1 h at room temperature. ITGB4, rather than integrin $\alpha_6\beta_4$ per se, was probed given ITGB4 is an obligate heterodimer with ITGA6 to form integrin $\alpha_6\beta_4$. Samples were counterstained with DAPI (4′, 6-diamidino-2-phenylindole dihydrochloride). Total fluorescent intensity in each field was quantified after accounting for secondary-only controls at constant microscope settings across all samples. Micrographs (×10) were obtained on an upright fluorescent microscope (DM 6B, Leica). Three fields of view (FOVs) were captured per sample (ImageJ, NIH) with at least five separate samples tested per group. Immunofluorescences are the gold-standard technique for HD formation by experimental biologists.[16]

2.3.2 | Keratinocyte proliferation

Samples were incubated for the given culture period (i.e., 1, 3, or 5 days), washed with PBS, and then incubated in CCK8 solution (Dojindo; 9:1 OK:CCK8 medium) for 3 h. Optical density (OD; $\lambda = 450$ nm) was evaluated using a plate reader (Synergy HT, Biotek). OD values were blanked to virgin CCK8 solution similarly incubated. Previously DAPI-stained samples were also quantified in terms of number of nuclei per field of view and converted to determine the number of nuclei per disk. Five samples were tested per group.

2.4 | Protein adsorption

2.4.1 | Bovine serum albumin adsorption

Samples were equilibrated in PBS for 10 min to form a hydrated surface layer. Then, samples were placed in 1.0% BSA (Pierce) in PBS and incubated at 37°C for 1 h. Samples were gently washed thrice in PBS to remove weakly bound BSA. Samples were then desorbed in 2% (v/v) Triton X-100 in PBS for 60 min total with 20 min of ultrasonication.[40] Protein concentration of the desorbed BSA was then determined using a commercially available kit (micro-BCA, Thermo-Fisher) with a standard curve and normalized to pGlass. Four samples were tested per group.

X-ray photoelectron spectroscopy was used to assess the BSA adlayer thickness; high resolution N1s spectra were obtained using the general XPS parameters as described, except with a pass energy of 190 eV and a step size of 0.1 eV. Intensity was converted to dehydrated thickness using a general relationship defined by others.[41] Three samples were tested per group.

2.4.2 | Fibrinogen adsorption

Samples were equilibrated in PBS for 10 min to form a hydrated surface layer. Then, samples were placed in 1 mg/ml fluorescently labeled Fg (isolated from human plasma; Invitrogen) in PBS and incubated at 37°C for 1 h.[42] Samples were gently washed thrice in PBS to remove weakly bound Fg. Fluorescent intensity of samples was then measured using an upright fluorescent microscope (DM 6B, Leica). Background-subtracted pixel intensities from non-adsorbed, newly synthesized pGlass were calculated and analyzed in ImageJ (NIH); three FOVs were captured from each of the three samples (ImageJ, NIH) tested per group. Data was normalized to pGlass.

2.5 | Statistical analysis

Mean values for different groups were compared with a one-way analysis of variance (ANOVA) followed by Tukey's HSD (honest significant difference) post hoc test. Dissimilar letters in figures indicate statistically significant differences between groups. GraphPad Prism 8.2.0 (GraphPad Software) was utilized to perform all statistical analysis. A p-value of <0.05 was considered statistically significant. Means and one standard deviation on the mean are reported. All biological experiments were independently repeated twice, one representative experiment is shown. Exact p-values may be found in Tables S1–S16.

3 | RESULTS

3.1 | Elemental composition and WCA

The water contact angle (WCA) for pGlass, —H, —CH_3, —NH_2, and —OH groups were 5.78° ± 1.15°, 42.02° ± 2.55°, 85.74° ± 0.99°, 65.73° ± 1.92°, and 34.92° ± 2.30°, respectively (Figure 1B, and Table S1). All differences were statistically significant. Notably, the pGlass group was the most hydrophilic surface and —CH_3 surfaces were the most hydrophobic. Overall schematics of the modified chemical structures of the glass surfaces after silanization with common biological groups are shown in Figure 1C.

X-ray photoelectron spectroscopy was used for determining surface elemental analysis to confirm synthesis of all modified glass surfaces. Si2s and Si2p (ca. 100 and 150 eV, respectively) and Sn3d (ca. 500 eV) were detected due to the glass bulk substrate. Detection of Si2p can be additionally attributed to presence of silane molecules on all silanized surfaces. Correspondingly, carbon (C1s) and oxygen (O1s) were also found on all surfaces after silanization (Figure 1D and Table 1). Furthermore, in surfaces modified with NH_2-terminated silanes, N1s was detected (ca. 400 eV). Figure S1 contains

TABLE 1 X-ray photoelectron spectroscopy (XPS) semiquantification of elemental composition (Mean at% ± standard deviation) of control and modified glass surfaces ($n = 3$)

Surface	C1s	N1s	O1s	Na1s	Si2p	Cl2p	Ca2p
pGlass	14.35 ± 0.80	0	64.10 ± 0.78	0.93 ± 0.35	19.93 ± 0.71	0.19 ± 0.29	0.51 ± 0.36
NH_2	30.98 ± 2.69	4.55 ± 0.73	47.18 ± 2.35	0.21 ± 0.30	15.86 ± 0.94	1.02 ± 0.47	0.20 ± 0.07
H	34.23 ± 1.95	0	46.39 ± 3.16	0.35 ± 0.40	17.88 ± 1.21	0.33 ± 0.22	0.83 ± 0.21
CH_3	35.75 ± 1.72	0	45.54 ± 1.17	0.11 ± 0.19	17.36 ± 1.21	0.06 ± 0.01	1.23 ± 0.08
OH	31 ± 1.50	0	53.14 ± 2.06	0.66 ± 0.43	14.94 ± 0.45	0.18 ± 0.21	0.09 ± 0.07

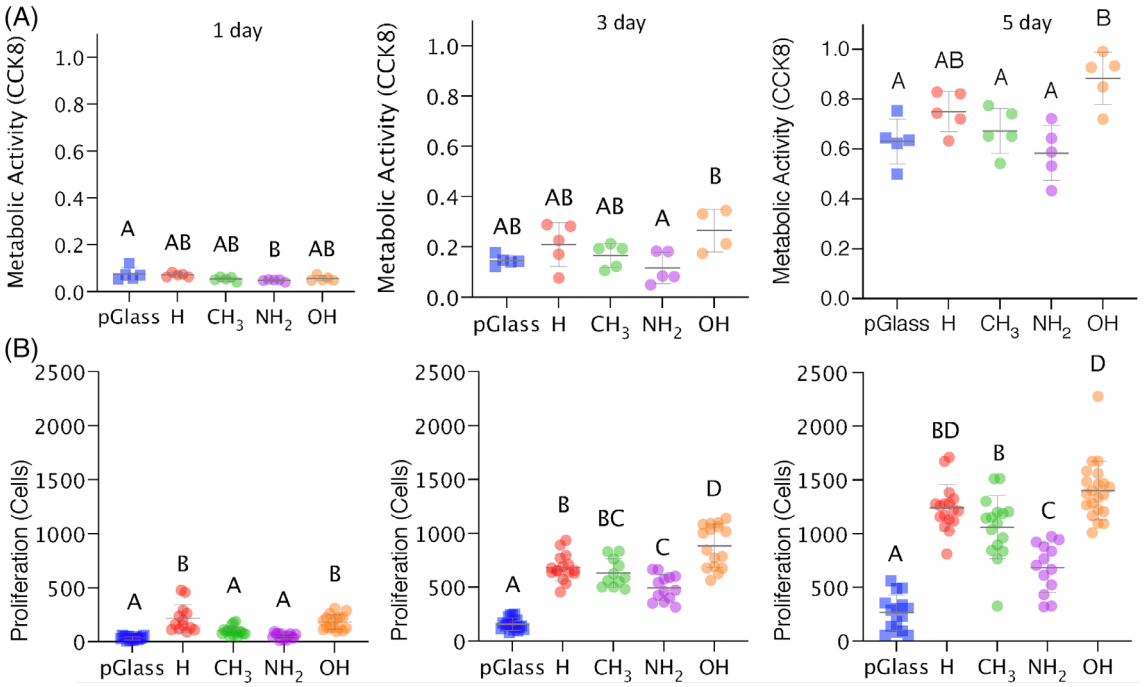

FIGURE 2 (A) CCK8 metabolic activity (optical density) analysis of oral keratinocytes (OKs) cultured on control and modified glass disks for 1, 3, and 5 days ($n = 5$). (B) Proliferation (number of DAPI-stained nuclei) of OKs on control and modified glass disks for 1, 3, and 5 days. Dissimilar letters indicate statistically significant differences between groups. Error bars represent standard deviation ($n = 5$; 3 FOVs per sample)

characteristics ATR-FTIR peaks for each group. Overall, these results confirmed the expected chemistries in the modified glass surfaces.

3.2 | Metabolic activity and OK proliferation

Oral keratinocyte (OK) metabolic activity was assessed as the first readout of oral keratinocyte behavior on surfaces with varied physico-chemistry. On the one hand, OKs on —OH and —H surfaces showed the highest CCK8 activity at every timepoint (Figure 2A, Tables S2–S4). This increased OKs CCK8 activity on the —OH and —H groups compared to the other groups was increasingly prominent from day 1 to day 5. On the other hand, CCK8 activity on —NH_2 surface was significantly lower compared to —OH by day 5.

DAPI staining to complementarily measure OKs proliferation at day 1, 3 and 5 revealed the highest number of cells on —OH and —H at all three timepoints (Figure 2B, Tables S5–S7), confirming the results from CCK8 activity. Indeed, by day 5, the number of DAPI-stained OKs on —NH_2 surface was significantly lower than all other modified surfaces.

3.3 | Bovine serum albumin and fibrinogen adsorption

The amount of two model proteins, BSA and Fg, adsorbed on the surfaces was then measured given the importance of sorbed proteins in mediating cell-surface interactions. There was significantly more Fg and BSA adsorbed on —H and —CH_3 modified surfaces than all other groups (Figure 3A,B, Tables S8 and S9). The pGlass and —OH surfaces showed the lowest BSA and Fg adsorption among all groups. No significant differences for BSA and Fg were observed between —NH_2 and —OH.

The thickness of the BSA adlayer on all groups was evaluated using XPS.[40] The —H and —CH_3 groups had the thickest BSA layer

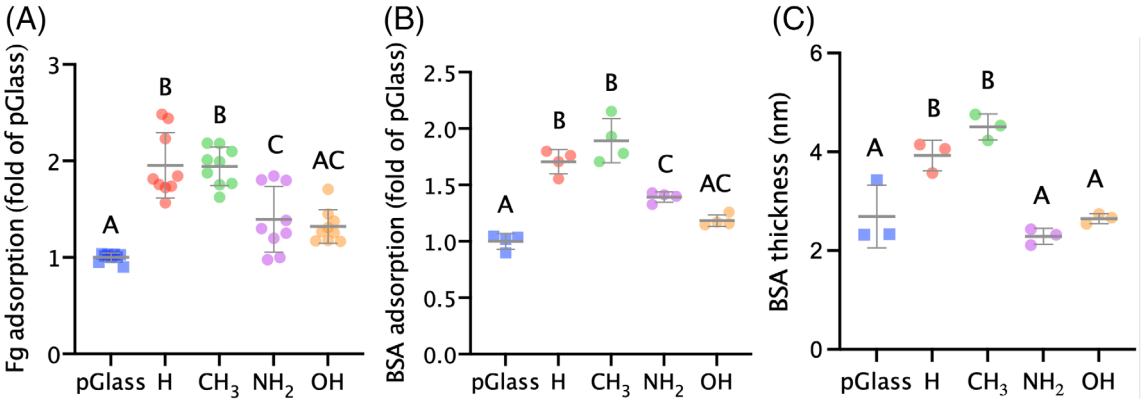

FIGURE 3 (A) Fibrinogen ($n = 3$; 3 FOVs per sample) and (B) Bovine serum albumin (BSA) and adsorption for control and modified glass disks. Values are normalized to pGlass ($n = 4$). (C) Thickness of the BSA layer formed on control and modified glass disks. Dissimilar letters indicate statistically significant differences between groups ($n = 3$). Error bars represent standard deviation

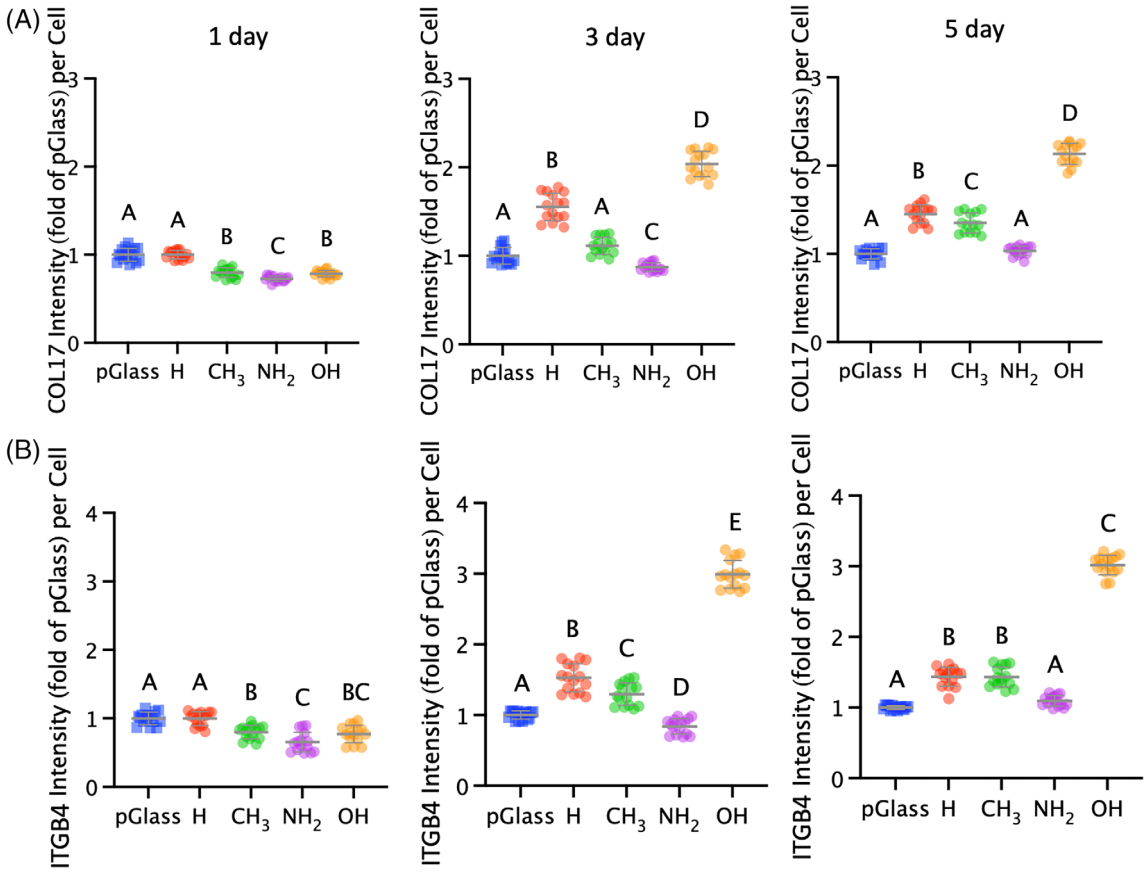

FIGURE 4 (A) Collagen XVII (COL17) expression levels by oral keratinocytes (OKs) on control and modified glass disks at 1, 3, and 5 days. Values are normalized to pGlass at each timepoint. (B) Integrin β_4 (ITGB4) expression levels by OKs on control and modified glass disks at 1, 3, and 5 days. Values are normalized to pGlass at each timepoint. Dissimilar letters indicate statistically significant differences between groups. Error bars represent standard deviation ($n = 5$; 3 FOVs per sample)

(Figure 3C, Table S10). Interestingly, even though —NH_2 adsorbed more BSA and Fg compared to pGlass, the BSA adlayer thickness on —NH_2 was less than pGlass, suggesting notable differences of protein conformation between these two surfaces.

3.4 | Hemidesmosome formation

We next quantified HD formation, the hallmark of robust keratinocyte attachment to teeth, using immunofluorescence against two HD

markers: ITGB4, expressed in early HD formation, and COL17, expressed in later HD maturation.[14,18,43] Although OKs on pGlass and —H groups showed the highest COL17 expressions at day 1 (Figure 4A, Tables S11–S13, and Figure S2), —OH surfaces induced a significantly higher expression of COL17 than all other tested surfaces by days 3 and 5. Conversely, pGlass and —NH_2 induced the lowest COL17 expression by OKs at days 3 and 5.

Similar results to COL17 were observed for ITGB4, OKs on pGlass and —H groups showing significantly higher expression of ITGB4 than on every other group at day 1, but —OH surfaces induced the significantly highest ITGB4 expression at day 3 and 5 (Figure 4B, Tables S14–S16, and Figure S3). In addition, as in the case of both ITGB4 and COL17 expression, pGlass and —NH_2 surfaces induced the lowest ITGB4 expression at days 3 and 5. Thus, the expression of COL17 and ITGB4 by OKs showed almost identical trends on all tested surfaces. Overall, the —OH surfaces induced the highest expression of both HD markers.

4 | DISCUSSION

There are no known correlations between basic physical–chemical properties of surfaces and induction of HD formation by OKs. We explore this here using model control and modified surfaces with organosilanes to offer well-ordered, robust coatings to modify surface physicochemical properties toward identifying ideal surface chemistries for desired cell phenotypes.[44,45] Successful synthesis of organosilane surfaces is supported by our WCA results being similar to previously reported surfaces with identical chemistries. WCA averages of 85.74°, 65.73° and 34.92° for —CH_3, —NH_2, and —OH, respectively, were comparable to values from previous studies measuring 107°–112° for —CH_3 groups, 26°–46° for —NH_2 groups, and 20°–30° for —OH groups.[25,26,37]

Our —OH organosilane-modified surfaces demonstrated the highest OKs proliferation and expression of both ITGB4 and COL17 HD markers compared to all other groups. Furthermore, while the —OH organosilane group performed best, the pGlass control—also rich in hydroxyls—was the lowest performing group. More specifically, pGlass and —OH groups feature abundant terminal hydroxyls, with the difference that hydroxyls are presented at the end of an alkyl chain in the —OH group. Of note, HD formation and OKs proliferation were significantly higher on —OH disks than pGlass disks, even though both presented similar levels of protein adsorption. We propose the physical–chemical environment of a polar surface favors HD formation by OKs and that the configuration (at the end of a hydrocarbon tail), in which the hydroxyl group is presented on the —OH surfaces, offers a certain degree of flexibility or diffusivity allowing the protein adlayer to exert the appropriate biological effects contrary to pGlass. Classical and recent work has shown the interplay between (1) the secreted and (2) adsorbed ECM (3) and/or surface receptor expression with the surface chemistry determines cell responses.[46,47] Polarity at short-range interactions (pGlass; no alkyl tail) appears to affect OKs and/or adsorbed or secreted matrix differently than longer range (—OH; with an alkyl tail) polar groups. Indeed, studies have shown that cellular responses to the same ligand are affected dramatically by immobilized ligand diffusivity.[48] Further work is necessary to better understand the potential role in ligand diffusivity in forming HD on surfaces. Interestingly, a positive correlation between metabolic activity and expression of HD markers COL17 and ITGB4 seems to be present; this is consistent with previous studies suggesting an intrinsic link among HD formation, proliferation, and the surface-dictated environment OKs interrogate and respond to.[22,37] Thus, control of HD formation through surface physicochemistry is a route to control cell behavior beyond HD, such as proliferation and potentially differentiation response that are linked to HD.[49] Future research could investigate this by looking at cell cycle or apoptosis markers in relationship to HD formation. Surface zeta analysis in future studies could directly show the differences in surface charge among different groups. Future surface characterization could be performed to comprehensively determine presence and quantify density of chemical groups using time-of-flight secondary ion mass spectrometry and/or colorimetric reactions.

Proteins and biomolecules that exist in human body solutions, such as blood and saliva, will be adsorbed by the modified surface of any device that will be implanted into the human body, dictating the performance of these surfaces. Relatively hydrophilic pGlass and —OH showed similarly low BSA and Fg adsorption and BSA thickness but a markedly different OKs response. On the other hand, hydrophobic modified —CH_3 titanium surfaces seem to adsorb more BSA and Fg than more hydrophilic modifications.[44,45] In accordance with the above, our —CH_3 group presented the highest levels of BSA and Fg adsorption. Similar results were shown for BSA thickness. This high BSA and Fg adsorption was associated with only moderate OK proliferation and HD formation. Overall, it could be assumed that BSA thickness, BSA and Fg adsorption are not correlated with the OKs proliferation nor HD formation on physicochemically modified surfaces. Our methods for studying adsorbed proteins had potential limitations, such as molecular physicochemical properties after fluorescent labeling can be different compared to native sequences or desorption and then quantification of biomolecules in solution may result in adsorption of said biomolecules to glassware and thus can alter the quantified signal.

Others have shown osteoblasts cultivated on Ti surfaces with preabsorbed BSA showed no difference on surface attachment compared to control Ti surfaces,[50] while attachment of dental pulp derived mesenchymal stem cells (DP-MSCs) was similar between Ti surfaces with fibronectin (Fn) coating and control Ti surfaces.[51] On the other hand, osteoblasts' adhesion was enhanced on Ti surfaces preadsorbed with Fn for 15 versus 180 min and non-coated Ti surfaces.[50] Thus, not all cell types seem to respond in the same way on BSA and Fg adsorption, which suggests that protein conformation, rather than amount, is a critical variable to examine in future work. This may relate to the reversibility of sorption. It appears that the irreversibility that a flat rigid substrate adsorbs more molecules, in contrast to a softer/more flexible monolayer of silanes, can impose that fewer conformational states of proteins are available for the cells to

interact with leading to favorable responses.[52] Future work is necessary to interrelate adsorbed biomolecule properties and HD upregulation. Indeed, this becomes important when many biomolecules are adsorbed simultaneously as surface properties guide which biomolecules preferentially adsorb[53,54] and/or their conformation. These relevant aspects of multi-protein adsorption and consequent biological implications have not been directly studied here.

Interestingly, the —OH group's average WCA of 34.92° is close to the WCA that has been related to the highest adhesion for human endothelial cells.[29] Others have identified a WCA of 24°–31° being ideal for osteoblast differentiation.[55,56] Yet others have shown that a WCA of 60°–80° is ideal for fibroblasts' focal adhesion formation.[57–59] We establish here that the relationship between keratinocyte HD formation and physicochemistry is distinct from other cells and phenotypes. Indeed, previously conducted studies with MSCs showed higher proliferation levels and focal adhesion formation on —OH and —NH_2 groups than —CH_3 group.[1] Similarly, MC3T3-E1 cells, osteoblast precursors, presented the highest amount of adhesion on —NH2 and —OH groups.[60] Moreover, —NH_2 surfaces seem to promote osteogenic differentiation of MSCs compared to other surfaces.[26–28] Similar results have been shown for dental pulp stem cells (hDPSCs).[3] Instead, we show HD formation by OKs was the lowest on the —NH_2 surface. Therefore, contrary to MSCs that prefer positively charged, polar hydrophilic surfaces, OKs prefer hydrophilic, polar, neutral surfaces for HD formation.

Other surfaces synthesized to upregulate HD have suggested the importance of physicochemistry. For example, differently modified Ti and zirconia (ZrO_2) implant surfaces have been tested for oral epithelial attachment *in vitro* and animals.[39,61–63] ZrO_2 implants showed comparable HD formation with Ti implants.[39] Other studies demonstrated that Ti implants hydrothermally treated with calcium chloride and zinc chloride had enhanced epithelial attachment compared to machined and hydrothermally treated with strontium chloride Ti implants.[60,62] In vitro studies presented that using ultraviolet light to modify Ti surfaces can enhanced HD formation of oral keratinocyte cells.[64] However, fundamental evaluation of systemically varied chemical groups and/or physicochemical modifications and their relationship to HD formation has not been performed until present. Our results will help unify disparate past in vitro results and provide guidance for future mechanistic studies and enhancement of soft tissue attachment around implants. The effectiveness of this HD-mediated biologic seal needs additional testing with animal studies and mechanistic studies focused on the role of extracellular matrix in HD formation in future work.[65]

5 | CONCLUSIONS

Organosilane-modified surfaces featuring a terminal —OH can increase OKs proliferation and HD formation. The favorable OKs response on the —OH surface appeared to not correlate with surface wettability or the effects of specific physical–chemical properties on the amount or thickness of the adlayer of adsorbed model proteins. These results highlight the potential of developing new surfaces to favor HD formation by simple chemical modifications and thus, advance peri-implantitis preventative strategies toward biologically-informed biomaterials.

ACKNOWLEDGMENTS

This study was supported by NIDCR R01DE026117, F30DE029105, and a 3M Science and Technology Fellowship. This content is solely the responsibility of the authors and does not necessarily represent the official views of the National Institutes of Health. CA acknowledges support from the Fundacio Bosch Aymerich through the FBA-BIST-UIC fellows program. Parts of this work were carried out in the Characterization Facility, University of Minnesota, which receives partial support from the NSF through the MRSEC (Award Number DMR-2011401) and the NNCI (Award Number ECCS-2025124) programs. Some images were created using BioRender. IBEC is a member of the CERCA Programme/Generalitat de Catalunya.

DATA AVAILABILITY STATEMENT

The data that support the findings of this study are available from the corresponding author upon reasonable request.

ORCID

Nicholas G. Fischer https://orcid.org/0000-0003-2230-5158
Conrado Aparicio https://orcid.org/0000-0003-2969-6067

REFERENCES

1. Yu S-J, Li Q-C, Shan W-Y, Hao Z-N, Li P, Liu J-F. Heteroaggregation of different surface-modified polystyrene nanoparticles with model natural colloids. *Sci Total Environ*. 2021;784:147190.
2. Boyan B. Role of material surfaces in regulating bone and cartilage cell response. *Biomaterials*. 1996;17:137-146.
3. Yu T-T, Cui F-Z, Meng Q-Y, et al. Influence of surface chemistry on adhesion and osteo/odontogenic differentiation of dental pulp stem cells. *ACS Biomater Sci Eng*. 2017;3:1119-1128.
4. Albrektsson T, Chrcanovic B, Östman P-O, Sennerby L. Initial and long-term crestal bone responses to modern dental implants. *Periodontol 2000*. 2017;73(1):41-50.
5. Atieh MA, Alsabeeha NHM, Faggion CM Jr, Duncan WJ. The frequency of Peri-implant diseases: a systematic review and meta-analysis. *J Periodontol*. 2012;84(11):1586-1598.
6. Renvert S, Persson GR, Pirih FQ, Camargo PM. Peri-implant health, peri-implant mucositis, and peri-implantitis: case definitions and diagnostic considerations: diagnostic criteria of peri-implant health and diseases. *J Periodontol*. 2018;89:S304-S312.
7. Schwarz F, Derks J, Monje A, Wang H-L. Peri-implantitis. *J Periodontol*. 2018;89:S267-S290.
8. Busscher HJ, van der Mei HC, Subbiahdoss G, et al. Biomaterial-associated infection: locating the finish line in the race for the surface. *Sci Transl Med*. 2012;4:153rv10. doi:10.1126/scitranslmed.3004528
9. Ma Y, Wang C, Li Y, et al. Considerations and caveats in combating ESKAPE pathogens against nosocomial infections. *Adv Sci (Weinh)*. 2020;7:1901872.
10. Marchetti C, Farina A, Cornaglia AI. Microscopic, immunocytochemical, and ultrastructural properties of Peri-implant mucosa in humans. *J Periodontol*. 2002;73:555-563.
11. Rompen E, Domken O, Degidi M, Farias Pontes AE, Piattelli A. The effect of material characteristics, of surface topography and of implant components and connections on soft tissue integration: a literature review. *Clin Oral Implants Res*. 2006;17:55-67.

12. Gibbs S. Department of Molecular Cell Biology and Immunology, O/2 building room 11E05, VU University Medical Centre, Amsterdam UMC, Amsterdam, The Netherlands. In: Roffel S, Meyer M, Gasser A, eds. *Biology of Soft Tissue Repair: Gingival Epithelium in Wound Healing and Attachment to the Tooth and Abutment Surface*. Vol 38. ECM; 2019:63-78.
13. Gould TRL, Brunette DM, Westsury L. The attachment mechanism of epithelial cells to titanium in vitro. *J Periodontal Res*. 1981;16: 611-616.
14. Borradori L, Sonnenberg A. Structure and function of hemidesmosomes: more than simple adhesion complexes. *J Invest Dermatol*. 1999;112:411-418.
15. Jones JC, Kurpakus MA, Cooper HM, Quaranta V. A function for the integrin alpha 6 beta 4 in the hemidesmosome. *Cell Regul*. 1991;2: 427-438.
16. Sonnenberg A, Calafat J, Janssen H, et al. Integrin alpha 6/beta 4 complex is located in hemidesmosomes, suggesting a major role in epidermal cell-basement membrane adhesion. *J Cell Biol*. 1991;113: 907-917.
17. Pora A, Yoon S, Windoffer R, Leube RE. Hemidesmosomes and focal adhesions treadmill as separate but linked entities during keratinocyte migration. *J Invest Dermatol*. 2019;139:1876-1888.e4.
18. Has C, Kern JS. Collagen XVII. *Dermatol Clin*. 2010;28:61-66.
19. Borradori L, Sonnenberg A. Hemidesmosomes: roles in adhesion, signaling and human diseases. *Curr Opin Cell Biol*. 1996;8:647-656.
20. Dowling J, Yu QC, Fuchs E. Beta4 integrin is required for hemidesmosome formation, cell adhesion and cell survival. *J Cell Biol*. 1996;134: 559-572.
21. Iglhaut G, Schwarz F, Winter RR, Mihatovic I, Stimmelmayr M, Schliephake H. Epithelial attachment and downgrowth on dental implant abutments – A comprehensive review: epithelial attachment and downgrowth on dental implant abutments. *J Esthet Restor Dent*. 2014;26:324-331.
22. Koidou VP, Argyris PP, Skoe EP, et al. Peptide coatings enhance keratinocyte attachment towards improving the peri-implant mucosal seal. *Biomater Sci*. 2018;6:1936-1945.
23. El-Ghannam A, Starr L, Jones J. Laminin-5 coating enhances epithelial cell attachment, spreading, and hemidesmosome assembly on Ti-6Al-4V implant materialin vitro. *J Biomed Mater Res*. 1998;41:30-40.
24. Fischer NG, Münchow EA, Tamerler C, Bottino MC, Aparicio C. Harnessing biomolecules for bioinspired dental biomaterials. *J Mater Chem B Mater Biol Med*. 2020;8:8713-8747.
25. Arima Y, Iwata H. Preferential adsorption of cell adhesive proteins from complex media on self-assembled monolayers and its effect on subsequent cell adhesion. *Acta Biomater*. 2015;26:72-81.
26. Bai B, He J, Li Y-S, Wang X-M, Ai H-J, Cui F-Z. Activation of the ERK1/2 signaling pathway during the osteogenic differentiation of mesenchymal stem cells cultured on substrates modified with various chemical groups. *Biomed Res Int*. 2013;2013:1-15.
27. Curran JM, Chen R, Hunt JA. Controlling the phenotype and function of mesenchymal stem cells in vitro by adhesion to silane-modified clean glass surfaces. *Biomaterials*. 2005;26:7057-7067.
28. Curran JM, Chen R, Hunt JA. The guidance of human mesenchymal stem cell differentiation in vitro by controlled modifications to the cell substrate. *Biomaterials*. 2006;27:4783-4793.
29. Metwally S, Stachewicz U. Surface potential and charges impact on cell responses on biomaterials interfaces for medical applications. *Mater Sci Eng C Mater Biol Appl*. 2019;104:109883.
30. Park J, Yu Y, Kim J, et al. Balanced effects of surface reactivity and self-association of bifunctional polyaspartamide on stem cell adhesion. *ACS Omega*. 2017;2:1333-1339.
31. Hong S, Ergezen E, Lec R, Barbee KA. Real-time analysis of cell–surface adhesive interactions using thickness shear mode resonator. *Biomaterials*. 2006;27:5813-5820.
32. Hormia M, Kononen M, Kivilahti J, Virtanen I. Immunolocalization of proteins specific for adhaerens junctions in human gingival epithelial cells grown on differently processed titanium surfaces. *J Periodontal Res*. 1991;26:491-497.
33. Corvino E, Pesce P, Mura R, Marcano E, Canullo L. Influence of modified titanium abutment surface on Peri-implant soft tissue behavior: a systematic review of in vitro studies. *Int J Oral Maxillofac Implant*. 2020;35:503-519.
34. Chen X, Sevilla P, Aparicio C. Surface biofunctionalization by covalent co-immobilization of oligopeptides. *Colloids Sur B*. 2013;107: 189-197.
35. Fischer NG, Moussa DG, Skoe EP, De Jong DA, Aparicio C. Keratinocyte-specific peptide-based surfaces for hemidesmosome upregulation and prevention of bacterial colonization. *ACS Biomater Sci Eng*. 2020;6:4929-4939.
36. Holmberg KV, Abdolhosseini M, Li Y, Chen X, Gorr S-U, Aparicio C. Bio-inspired stable antimicrobial peptide coatings for dental applications. *Acta Biomater*. 2013;9:8224-8231.
37. Bush KA, Driscoll PF, Soto ER, Lambert CR, McGimpsey WG, Pins GD. Designing tailored biomaterial surfaces to direct keratinocyte morphology, attachment, and differentiation. *J Biomed Mater Res A*. 2009;90A:999-1009.
38. Dickson MA, Hahn WC, Ino Y, et al. Human keratinocytes that express hTERT and also bypass a p16 INK4a -enforced mechanism that limits life span become immortal yet retain normal growth and differentiation characteristics. *Mol Cell Biol*. 2000;20:1436-1447.
39. Ayukawa Y, Atsuta I, Moriyama Y, Jinno Y, Koyano K. Localization of integrin beta-4 subunit at soft tissue–titanium or zirconia interface. *J Clin Med*. 2020;9:3331.
40. Chen C, Wu J, Weir M, et al. Dental composite formulation design with bioactivity on protein adsorption combined with crack-healing capability. *J Funct Biomater*. 2017;8:40.
41. Ray S, Shard AG. Quantitative analysis of adsorbed proteins by X-ray photoelectron spectroscopy. *Anal Chem*. 2011;83:8659-8666.
42. Liu S, Ma J, Xu L, et al. An electrospun polyurethane scaffold-reinforced zwitterionic hydrogel as a biocompatible device. *J Mater Chem B Mater Biol Med*. 2020;8:2443-2453.
43. Powell AM, Sakuma-Oyama Y, Oyama N, Black MM. Collagen XVII/BP180: a collagenous transmembrane protein and component of the dermoepidermal anchoring complex. *Clin Exp Dermatol*. 2005; 30:682-687.
44. Hasan A, Waibhaw G, Pandey LM. Conformational and organizational insights into serum proteins during competitive adsorption on self-assembled monolayers. *Langmuir*. 2018;34:8178-8194.
45. Hasan A, Saxena V, Pandey LM. Surface functionalization of Ti6Al4V via self-assembled monolayers for improved protein adsorption and fibroblast adhesion. *Langmuir*. 2018;34:3494-3506.
46. Loebel C, Mauck RL, Burdick JA. Local nascent protein deposition and remodelling guide mesenchymal stromal cell mechanosensing and fate in three-dimensional hydrogels. *Nat Mater*. 2019;18:883-891.
47. Coelho NM, González-García C, Salmerón-Sánchez M, Altankov G. Arrangement of type IV collagen on NH2 and COOH functionalized surfaces. *Biotechnol Bioeng*. 2011;108:3009-3018.
48. Yu L, Hou Y, Xie W, et al. Ligand diffusion enables force-independent cell adhesion via activating α5β1 integrin and initiating rac and RhoA signaling. *Adv Mater*. 2020;32:2002566.
49. Walko G, Castañón MJ, Wiche G. Molecular architecture and function of the hemidesmosome. *Cell Tissue Res*. 2015;360:363-378.
50. Yang Y, Cavin R, Ong JL. Protein adsorption on titanium surfaces and their effect on osteoblast attachment. *J Biomed Mater Res*. 2003;67A: 344-349.
51. Dolatshahi-Pirouz A, Jensen T, Kraft DC, et al. Fibronectin adsorption, cell adhesion, and proliferation on nanostructured tantalum surfaces. *ACS Nano*. 2010;4:2874-2882.

52. Ouberai MM, Xu K, Welland ME. Effect of the interplay between protein and surface on the properties of adsorbed protein layers. *Biomaterials*. 2014;35:6157-6163.
53. Buck E, Lee S, Stone LS, Cerruti M. Protein adsorption on surfaces functionalized with COOH groups promotes anti-inflammatory macrophage responses. *ACS Appl Mater Interfaces*. 2021 Feb 17;13(6):7021-7036.
54. Buck E, Lee S, Gao Q, et al. The role of surface chemistry in the Osseointegration of PEEK implants. *ACS Biomater Sci Eng*. 2022 Apr 11;8(4):1506-1521.
55. Chang HI, Wang Y. Cell responses to surface and architecture of tissue engineering scaffolds. *Regenerative Medicine and Tissue Engineering – Cells and Biomaterials*. InTech; 2011.
56. Yildirim ED, Besunder R, Pappas D, Allen F, Güçeri S, Sun W. Accelerated differentiation of osteoblast cells on polycaprolactone scaffolds driven by a combined effect of protein coating and plasma modification. *Biofabrication*. 2010;2:014109.
57. Groth T, Altankov G. Studies on cell-biomaterial interaction: role of tyrosine phosphorylation during fibroblast spreading on surfaces varying in wettability. *Biomaterials*. 1996;17:1227-1234.
58. Tamada Y, Ikada Y. Effect of preadsorbed proteins on cell adhesion to polymer surfaces. *J Colloid Interface Sci*. 1993;155:334-339.
59. Wei J, Igarashi T, Okumori N, et al. Influence of surface wettability on competitive protein adsorption and initial attachment of osteoblasts. *Biomed Mater*. 2009;4:045002.
60. Keselowsky BG, Collard DM, García AJ. Surface chemistry modulates focal adhesion composition and signaling through changes in integrin binding. *Biomaterials*. 2004;25:5947-5954.
61. Zhou X, Atsuta I, Ayukawa Y, et al. Effects of different divalent cation hydrothermal treatments of titanium implant surfaces for epithelial tissue sealing. *Materials (Basel)*. 2020;13:2038.
62. Narimatsu I, Atsuta I, Ayukawa Y, et al. Epithelial and connective tissue sealing around titanium implants with various typical surface finishes. *ACS Biomater Sci Eng*. 2019;5:4976-4984.
63. Rausch MA, Shokoohi-Tabrizi H, Wehner C, et al. Impact of implant surface material and microscale roughness on the initial attachment and proliferation of primary human gingival fibroblasts. *Biology (Basel)*. 2021;10:356.
64. Nakhaei K, Ishijima M, Ikeda T, Ghassemi A, Saruta J, Ogawa T. Ultraviolet light treatment of titanium enhances attachment, adhesion, and retention of human oral epithelial cells via decarbonization. *Materials (Basel)*. 2020;14:151.
65. Fischer NG, Kobe AC, Dai J, et al. Tapping basement membrane motifs: Oral junctional epithelium for surface-mediated soft tissue attachment to prevent failure of percutaneous devices. *Acta Biomater*. 2022;141:70-88.

SUPPORTING INFORMATION

Additional supporting information can be found online in the Supporting Information section at the end of this article.

How to cite this article: Raptopoulos M, Fischer NG, Aparicio C. Implant surface physicochemistry affects keratinocyte hemidesmosome formation. *J Biomed Mater Res*. 2023;111(7):1021-1030. doi:10.1002/jbm.a.37486